Integration of Ganglioside GT_{1b} Receptor into DPPE and DPPC Phospholipid Monolayers: An X-Ray Reflectivity and Grazing-Incidence Diffraction Study

C. E. Miller,* D. D. Busath,† B. Strongin,† and J. Majewski*
*Manuel Lujan Neutron Scattering Center, Los Alamos National Laboratory, Los Alamos, New Mexico, and †Department of Physiology and Developmental Biology, Brigham Young University, Provo, Utah

ABSTRACT Using synchrotron grazing-incidence x-ray diffraction (GIXD) and reflectivity, the in-plane and out-of-plane structures of mixed-ganglioside GT_{1b}-phospholipid monolayers were investigated at the air-liquid interface and compared with monolayers of the pure components. The receptor GT_{1b} is involved in the binding of lectins and toxins, including botulinum neurotoxin, to cell membranes. Monolayers composed of 20 mol % ganglioside GT_{1b}, the phospholipid dipalmitoyl phosphatidylethanolamine (DPPE), and the phospholipid dipalmitoyl phosphatidylcholine (DPPC) were studied in the gel phase at 23°C and at surface pressures of 20 and 40 mN/m, and at pH 7.4 and 5. Under these conditions, the two components did not phase-separate, and no evidence of domain formation was observed. The x-ray scattering measurements revealed that GT_{1b} was intercalated within the host DPPE/DPPC monolayers, and slightly expanded DPPE but condensed the DPPC matrix. The oligosaccharide headgroups extended normally from the monolayer surfaces into the subphase. This study demonstrated that these monolayers can serve as platforms for investigating toxin membrane binding and penetration.

INTRODUCTION

Cell membranes in the immune system, nervous system, placenta, and transformed malignant cancer cells are rich in glycolipids (1). Their complex biochemical and biophysical properties (1,2), and their place in the lipidome (3), were recently reviewed. Because of their extensive hydrogen-bonding capacity, they are interesting both as potential nucleation sites for lateral organization in the plasmalemma, and as receptors or ligands for binding extracellular agents.

Ganglioside lipids consist of a sphingosine base (with its hydrophobic tail) linked by a peptide bond to a fatty acid and also to a chain of highly soluble cyclic sugar residues (e.g., glucose or galactose) with one (GM), two, or three (GT) sialic-acid branches (4). The neutral sugar groups and negatively charged sialate residues constitute highly soluble hydrophilic headgroups on the diacyl lipids, such that the critical micelle concentrations for mono-, di-, and trisialogangliosides are 10–40 nM (5), higher than those of similar phospholipids, e.g., ~0.5 nM for dipalmitoyl phosphatidylcholine (6). Ganglioside lipids partition into rafts (7), presumably because of their saturated ceramide tails. The aggregative properties of ganglioside lipids were thoroughly reviewed (5).

To highlight their importance in a large variety of cellular processes, ganglioside lipids bind to lectins, serving as immunological and cell-adhesion receptors. They participate in cell signaling, oncogenesis, and cell differentiation (8–16). They are important in placentation and nerve growth, and they participate in myelin stability and nerve regeneration (17,18). Viral entry and budding also involve protein associations with ganglioside lipids (19–22).

Ganglioside lipids are important to the mechanisms of how bacterial toxins bind and gain entry to the interior of cells. Cholera toxin (23–25) binds specifically to GM_1, whereas botulinum neurotoxin type A (26–35) and tetanus toxin (28) bind strongly to trisialogangliosides.

Ganglioside lipid headgroups are known to be perpendicular to the membrane, based on vesicle electrophoresis, atomic force microscopy, and molecular dynamics simulations (1). Recently, neutron and x-ray reflectometry were used to characterize GM_1-containing monolayer structures (36,37). Moreover, x-ray reflectometry (XR) has the ability to characterize the electron-density profile normal to the membrane surface.

We present x-ray scattering studies of GT_{1b}, a prominent neuronal glycolipid, which is the primary ganglioside receptor for botulinum neurotoxin type A, and is important in most or all of the processes mentioned above. The receptor GT_{1b} is probably surrounded in the cell-membrane raft by saturated lipids such as sphingomyelin. As an approximation of this environment, we used monolayers of dipalmitoyl phosphatidylethanolamine (DPPE) or dipalmitoyl phosphatidylcholine (DPPC), which, with their saturated tails, are likely to be similar in structure to other raft lipids. By varying the surface pressure, we examined the tail-packing properties under both relatively tight and loosely packed conformations. In addition, the use of DPPE and DPPC enabled the use of grazing-incidence x-ray diffraction (GIXD). This technique is very valuable in the determination of in-plane structural parameters and the evaluation of detailed molecular intercalation and spacing properties of the lipid mixture. Using XR and GIXD, we evaluated the thickness of the sugar

Submitted December 27, 2007, and accepted for publication June 12, 2008.

Address reprint requests to J. Majewski, Lujan Neutron Scattering Center, Los Alamos National Laboratory, Los Alamos, New Mexico. E-mail: jarek@lanl.gov.

Editor: Thomas J. McIntosh.

0006-3495/08/10/3278/09 $2.00

doi: 10.1529/biophysj.107.128538

headgroup layer quantitatively, and determined how headgroup structure and spacing change when DPPE or DPPC molecules are interposed between GT_{1b} molecules. We also addressed the question of how the presence of GT_{1b} molecules affects the extent of in-plane order of host DPPE or DPPC molecules. The results bespeak the homogeneity of GT_{1b} distribution in such a bilayer, and lay the groundwork for studies of more raft-like mixtures of lipids. Moreover, these studies demonstrate that these monolayers are stable up to 20 mol % of GT_{1b}. This relatively high concentration of GT_{1b} will maximize interactions of proteins that associate with GT_{1b}, making these monolayers an ideal platform for investigating toxin membrane-binding and penetration.

EXPERIMENTAL SECTION

Materials

Lipid monolayers were composed using DPPE (1,2-dipalmitoyl-*sn*-glycero-3-phosphoethanolamine), DPPC (1,2-dipalmitoyl-*sn*-glycero-3-phosphocholine), and trisialoganglioside GT_{1b} (Cer-Glc-Gal(NeuAc-NeuAc)-GalNAc-Gal-NeuAc). The DPPE and DPPC were obtained from Avanti Polar Lipids (Alabaster, AL), and GT_{1b} (catalog No. G3767) was obtained from Sigma (St. Louis, MO). All lipids were used without further purification. The chemical structure of each lipid is presented in Fig. 1. Lipids were dissolved in chloroform/methanol 90:10 (~1.2 mg/mL), and deposited on an H_2O buffer subphase (pH 7.4 or 5). Buffer chemicals were purchased from Sigma, and prepared using Millipore (Billerica, MA) H_2O with 170 mM NaCl, 8.3 mM sodium phosphate. The pH was adjusted by titration with NaOH or HCl. All surface pressure-area isotherms were performed on a Nima Langmuir trough (Nima Technology, Coventry, England) at 23°C (±1°C) at a compression rate of 10 cm^2/min. All isotherm results are the averages of at least three measurements, and deviations were <5%.

X-ray reflectivity

The theory of XR and GIXD was presented in detail elsewhere (38–41), and the scattering geometries were also previously illustrated (41,42), so only a short discussion will be given here. All synchrotron x-ray measurements were performed using the liquid surface diffractometer at the BW1 (undulator) beam line at Hamburger Synchrotronstrahlungslabor (HASYLAB), Deutsches Elektronen-Synchrotron (DESY) (Hamburg, Germany). A temperature-controlled Langmuir trough, equipped with a Wilhelmy balance for surface-pressure measurements and a motorized barrier for surface-area variation, was mounted on the diffractometer. The trough was enclosed in a sealed, helium-filled canister where the oxygen level was constantly maintained at <2%, to minimize beam damage. The synchrotron x-ray beam was monochromated to a wavelength of $\lambda \sim 1.304$ Å by the (200) Bragg reflection from a beryllium monochromator crystal in Laue geometry. By tilting the reflecting crystal planes out of the vertical plane, the monochromatic beam was deflected down to impinge on the horizontal liquid surface at a shallow glancing angle.

Reflectivity, R, is defined as the ratio of the intensity of x-rays specularly reflected from a surface relative to that of the incident x-ray beam. When measured as a function of wave-vector transfer ($q_z = |k_{out} - k_{in}| = 4\pi \sin\alpha/\lambda$, where α is the grazing angle, and λ is the wavelength of the x-ray beam), the reflectivity curve contains information on the sample-normal profile of the in-plane average of the electron density. Reflectivities with q_z values from 0.01–0.8 $Å^{-1}$ were measured using a NaI scintillation detector, and reasonable statistics were obtained for values of $R \geq 10^{-10}$. Typical scanning times for this q_z range were 30 min. The absolute reflectivity was derived by subtracting the background, followed by normalization to the incident beam flux. The data were reduced and plotted as R/R_F versus the perpendicular scattering vector, q_z. Division by Fresnel reflectivity, R_F, increases the visibility of the reflectivity profile by removing the sharp q_z^{-4} decrease of the reflectivity attributable to Fresnel's law. The error bars in the data represent statistical errors in the measurements (standard deviation, $\pm\sigma_R$).

Analysis of the measured reflectivity curves was performed using a model-free approach (43–45). In this method, the electron-density profile was parameterized using cubic B-splines. The coefficients in the series were determined by constrained nonlinear least-squares methods, in which the smoothest solution with the lowest χ^2 was chosen. We present a family of models deviating by a maximum of 5% of the minimum χ^2. As a result, there is a broadening of the electron-density distribution, which is a measure of the uncertainty in the real-space structure. In this manner, detailed information on electron-density distribution in the direction normal to the interface was determined. Fluorescence microscopy measurements (data not shown) showed a homogenous monolayer structure, with no visible domains.

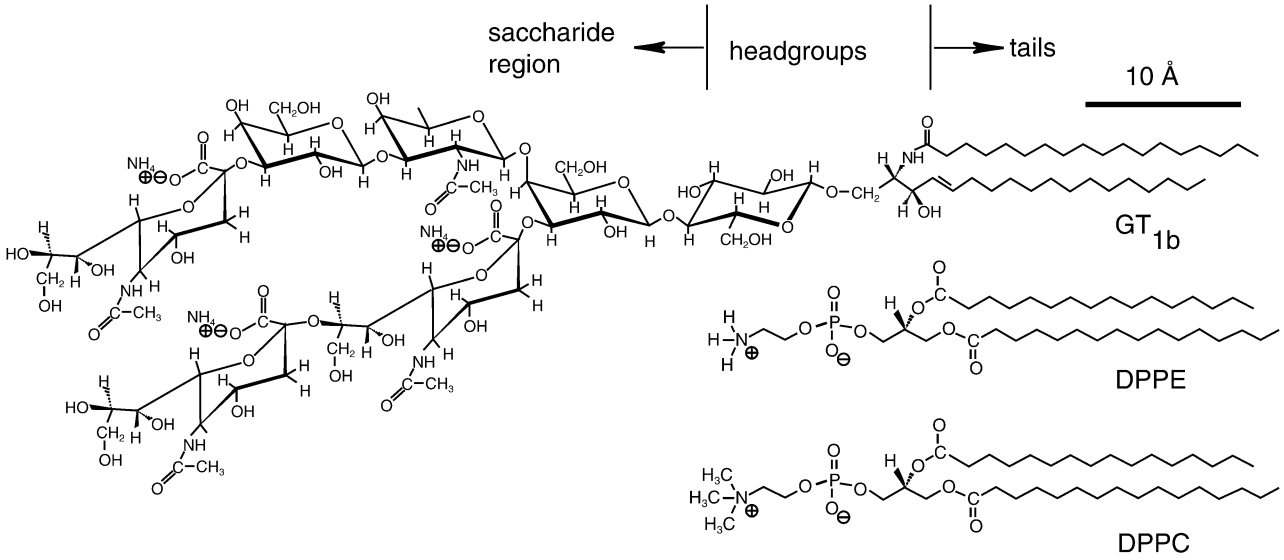

FIGURE 1 Chemical structure of GT_{1b}, DPPE, and DPPC. A bar of length 10 Å is shown for reference. The saccharide region of GT_{1b} is not drawn to scale, for better visibility of its chemical structure.

Grazing-incidence x-ray diffraction

Grazing-incidence x-ray diffraction can provide information about any lateral ordering within the system, comparable to wide-angle x-ray diffraction and grazing-incidence small-angle x-ray scattering (46–49). For the GIXD experiments, the x-ray beam was adjusted to strike the surface at an incident angle of 0.11°, which corresponds to $q_z = 0.85\, q_c$, where $q_c = 0.0219$ Å^{-1} is the critical scattering vector for total external reflection from the buffered liquid subphase. At this angle, the incident wave is totally reflected, whereas the refracted wave becomes evanescent, traveling along the liquid surface. Such a configuration maximizes surface sensitivity. The dimension of the x-ray beam footprint on the liquid surface was ~2 mm × 50 mm. For in-plane diffraction measurements, a Soller collimator (JJ X-ray, Liseleje, Denmark), consisting of closely spaced vertical plates, was placed before a vertical, one-dimensional position-sensitive detector with vertical acceptance $0 < q_z < 1.2$ Å^{-1}, yielding a lateral resolution of $\Delta q_{xy} = 0.0084$ Å^{-1}.

From three-dimensional (3D) crystals, strong diffraction from a set of crystal planes with interplanar spacing d occurs only when the Bragg law ($n\lambda = 2d\sin\theta$) is obeyed. More precisely, diffraction occurs only when the scattering vector, q, coincides with points of the reciprocal 3D lattice with integer Miller indices (h, k, l), giving rise to Bragg spots. In our two-dimensional (2D) systems, the monolayers are a mosaic of 2D crystals with random orientation about the direction normal to the subphase, and can therefore be described as 2D powders. Because of the lack of restriction on the scattering vector component q_z along the direction normal to the 2D crystal, Bragg scattering extends as continuous Bragg rods in reciprocal space (see Als-Nielsen et al. (38)).

The scattered intensity was measured by scanning over a range of horizontal scattering vectors

$$q_{xy} \equiv (q_x^2 + q_y^2)^{\frac{1}{2}} = \frac{2\pi}{\lambda}[\cos^2(\alpha_i) + \cos^2(\alpha_f) - 2\cos(\alpha_i)\cos(\alpha_f)\cos2\theta_{xy})]^{\frac{1}{2}}, \cong \frac{2\pi}{\lambda}[1 + \cos^2(\alpha_f) - 2\cos(\alpha_f)\cos2\theta_{xy})]^{\frac{1}{2}}$$

where $2\theta_{xy}$ is the angle between the incident and diffracted beam projected onto the horizontal plane, q_{xy} is the combination of horizontal components q_x and q_y, and α_i and α_f are the incident and the scattered angles, respectively (38,39). Note that only for $\alpha_f \approx 0$ is $q_{xy} \approx (4\pi/\lambda)\sin(2\theta_{xy}/2)$. Bragg peaks are the intensity resolved in the q_{xy}-direction and integrated over channels along the z-direction in the position-sensitive detector. Conversely, the Bragg rod profiles are the intensity resolved in the q_z-direction (i.e., along $q_z = 2\pi/\lambda(\sin\alpha_i + \sin\alpha_f) \approx 2\pi/\lambda\sin\alpha_f$) and integrated over the q_{xy} range of the Bragg peak. The configuration of the position-sensitive detector (described above) allowed Bragg-peak and Bragg-rod measurements to be made simultaneously. The position of the maxima of the Bragg peaks, q_{xy}^{max}, allows the determination of the repeat distances $d = 2\pi/q_{xy}$ of the 2D lattice. From the widths of the peaks, corrected for the instrument resolution, it is possible to determine the 2D crystalline in-plane coherence length, L_{xy} (the average distance in the direction of the reciprocal lattice vector $q$xy over which there is ''near-perfect'' crystallinity). The intensity distribution along the Bragg rod was analyzed to determine the direction and magnitude of the molecular tilt (measured from the water-surface normal), the coherently scattering length of the molecule, Lc, and the magnitude of molecular motion or surface roughness, σ, of the crystallite (Debye-Waller factor).

RESULTS

Surface pressure-area isotherms

Pressure-area isotherms for GT_{1b}, DPPE, DPPC, 1:4 mol % GT_{1b}/DPPE, and 1:4 mol % GT_{1b}/DPPC are shown in Fig. 2. As shown in the 100% GT_{1b} isotherm, the large size of the GT_{1b} headgroup caused a nonzero surface pressure even at areas per molecule above 100 Å^2. This behavior is typical for a fluid-phase monolayer with a large, bulky headgroup (50). The pure DPPE monolayer had a much sharper pressure increase, distinctive for a solid-phase monolayer. The GT_{1b}/DPPE lipid monolayer could almost be superimposed on the isotherm of pure DPPE. If there were significant phase separation of the two components, the expected isotherm would have been a linear combination of the pure DPPE and pure GT_{1b} isotherm. This indicates that GT_{1b} molecules, up to a mole fraction of 20%, are incorporated into the DPPE matrix and do not significantly disturb the packing of DPPE molecules. However, the 1:4 mol % GT_{1b}/DPPC monolayer showed a condensing effect, designated as a lower surface pressure, in the liquid-solid phase transition. A similar observation was observed in GM_1/DPPC mixtures (51). Above a surface pressure of 10 mN/m, the isotherms of pure DPPC and 1:4 mol % GT_{1b}/DPPC are almost identical.

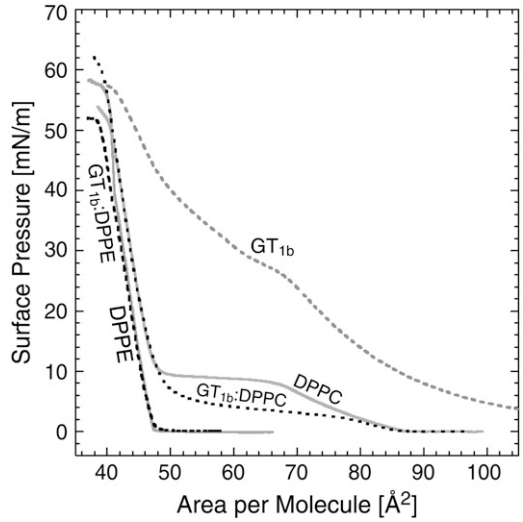

FIGURE 2 Pressure-area isotherms for GT_{1b}, DPPE, DPPC, 1:4 mol % GT_{1b}/DPPE, and 1:4 mol % GT_{1b}/DPPC. Isotherm of GT_{1b}/DPPE lipid monolayer could almost be superimposed on isotherm of pure DPPE. This indicated that GT_{1b} molecules, up to a mole fraction of 20%, are incorporated into DPPE matrix and do not significantly disturb the packing of DPPE. However, the 1:4 mol % GT_{1b}/DPPC monolayer showed a condensing effect, designated as a lower surface pressure, in the liquid-solid phase transition. Above surface pressures of 10 mN/m, isotherms of DPPC and 1:4 mol % GT_{1b}/DPPC are almost identical.

Reflectivity analysis

Reflectivity measurements of lipid monolayers at the air-liquid interface enabled a determination of the average electron-density profile normal to the interface. The experimentally measured, Fresnel-divided reflectivity profiles for a pure GT_{1b} monolayer, a pure DPPE monolayer, and a 1:4 mol % GT_{1b}/DPPE monolayer on an H_2O/buffer subphase (pH 7.4, 20 mN/m) are shown in Fig. 3 *a*. More quantitative de-

tails were obtained using cubic B-spline fits to ''invert'' the reflectivity profile into real-space structures. The corresponding electron-density profiles, $\rho(z)$, obtained from the cubic B-spline fits, are shown in Fig. 3 *b* (*solid curves*). The family of models deviating by a maximum of 5% of the minimum χ^2 is shown for each monolayer, which reflects the uncertainty in the real-space structure.

In Fig. 3 *b*, the headgroup and tail region of pure DPPE are distinguishable with a maximum headgroup electron density of $1.36\rho_{subphase}$, in agreement with previous studies of similar systems (52,53). The electron density of the tail region corresponds to an average area per molecule of ~43 Å^2. The electron-density profile of the 1:4 GT_{1b}/DPPE monolayer was similar to pure DPPE, with the addition of electron density at larger depth attributable to the GT_{1b} saccharide region, clearly extending (20–25 Å) into the liquid subphase from the DPPE headgroup. The profile also reveals a lower electron density of the saccharide region at a depth of ~29 Å, consistent with the single sugar chain in the GT_{1b} chemical structure. For the mixed monolayer, the alkyl tail region had the same thickness, roughness, and electron density as pure DPPE, indicating that an out-of-plane staggering of the two components did not occur.

In the case of pure GT_{1b} at 20 mN/m, the total length (30–35 Å, measured between inflection points on the electron-density distribution) was significantly less than expected from the molecular structure. Because of the large size of the hydrophilic saccharide headgroup at large area per molecule, the saccharide region can adopt many conformations that do not fully extend into the subphase. At higher surface pressures (~35 mN/m), the reduction in area per molecule caused the saccharide region to extend and the total thickness of pure GT_{1b} to be equivalent to the total thickness of the GT_{1b}/DPPE monolayer (data not shown). Pure GT_{1b} was unstable at surface pressures >35 mN/m.

Based on a reflectivity analysis, a 20 mol % of GT_{1b} within a DPPE matrix provided sufficient spacing between GT_{1b} molecules laterally, and allowed the GT_{1b} receptor to assume full extension from the membrane surface. On average, GT_{1b} molecules are ~15–20 Å apart along any particular direction, which does not significantly disturb the packing of the host lipid matrix. There were no significant structural changes in the equivalent monolayers at 20 mN/m and at pH 5 (data not shown), suggesting sufficient shielding by mobile ions from the bath at pH 7.4. At pH 5, the sialic-acid residues in the GT_{1b} saccharide region are expected to have a neutral charge. There were also no remarkable changes in the real-space structure at a surface pressure of 40 mN/m, except for a slight lengthening of the tail region, presumably because of a near-zero molecular tilt imposed by a decrease in area per molecule.

Fig. 4 *a* shows the experimentally measured, Fresnel-divided reflectivity profiles for a DPPC monolayer and a 1:4 GT_{1b}/DPPC monolayer, compared with the same GT_{1b} monolayer in Fig. 3, on an H_2O/buffer subphase (pH 7.4, 20 mN/m). The corresponding electron-density profiles, $\rho(z)$, obtained from the cubic B-spline fits, are shown in Fig. 4 *b* (*solid curves*).

There are two key differences between DPPC-based monolayers compared with DPPE and its mixture: (1), For pure DPPC, the electron density of the headgroup region was $1.28\rho_{subphase}$, compared with $1.36\rho_{subphase}$ in the case of the pure DPPE. This decrease is attributable to the greater volume of the DPPC headgroup (54). (2), The larger volume of the DPPC headgroups also causes the DPPC tails to have greater tilt relative to the surface normal (48,55). This is evident in the electron-density profile as a shorter thickness of the tail region compared with DPPE. The total thickness of the pure DPPC monolayer (~23 Å) is approximately half of a DPPC bilayer (47.0 Å) in the $L_{\beta'}$ phase at 20°C (57). The distance from the end of the hydrocarbon chain to the maximum headgroup

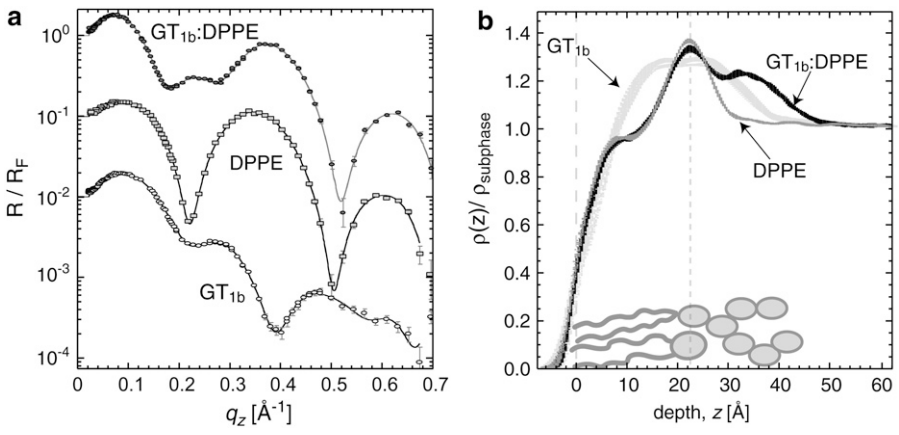

FIGURE 3 X-ray reflectivity results for monolayers of pure GT_{1b}, DPPE, and 1:4 mol % GT_{1b}/DPPE at pH 7.4 and surface pressure of 20 mN/m. (*a*) Measured reflectivity plotted as $R/R_{Fresnel}$ vs. q_z. Error bars for reflectivity data represent statistical errors in these measurements. Measured data are represented as symbols, and solid lines represent fits with lowest χ^2. Curves were vertically offset by factors of 10 for clarity. (*b*) Electron-density profiles for pure GT_{1b}, DPPE, and 1:4 mol % GT_{1b}/DPPE monolayers at 20 mN/m on water/buffer subphase. The thickness of electron-density profiles, corresponding to reflectivity fits with χ^2 values at no more than 5% of the minimal value, represents uncertainty in real-space structure. Electron densities $\rho(z)$ are normalized to the electron density of water with buffer, $\rho_{subphase} = 0.339\ e^-/Å^{-3}$. In the electron-density profile of the GT_{1b}/DPPE monolayer, the saccharide group of GT_{1b} is clearly evident as a large electron-density increase extending ~20 Å into the subphase from the DPPE headgroup region (at ~22 Å; *dashed line*). (*b*) Illustration of one DPPE molecule and one GT_{1b} molecule in their approximate orientation at the liquid surface. Dashed line at depth equal to 0 Å represents average position of alkyl tails/air interface.

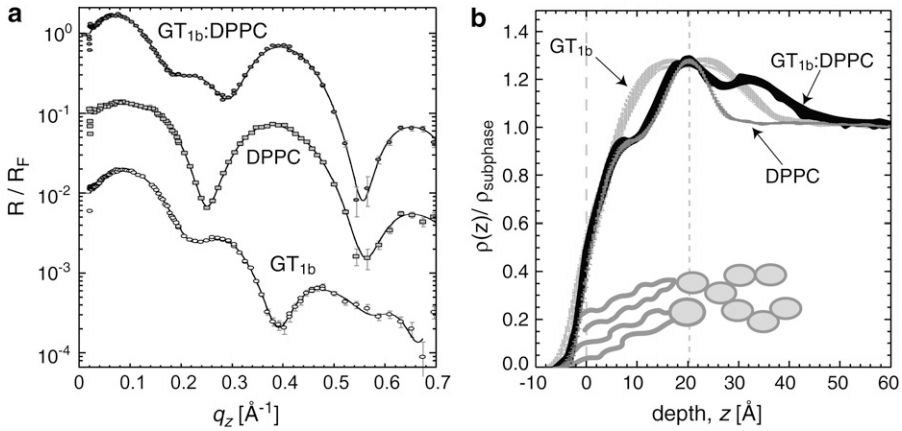

FIGURE 4 X-ray reflectivity results for monolayers of pure GT_{1b}, DPPC, and 1:4 mol % GT_{1b}/DPPC at pH = 7.4 and surface pressure of 20 mN/m. (*a*) Measured reflectivity, plotted as $R/R_{Fresnel}$ vs. q_z. Error bars for reflectivity data represent statistical errors in these measurements. Measured data are represented as symbols, and solid lines represent fits with the lowest χ^2. Curves were vertically offset by factors of 10 for clarity. (*b*) Electron-density profiles for pure GT_{1b}, DPPC, and 1:4 mol % GT_{1b}/DPPC monolayers at 20 mN/m on a water/buffer subphase. Electron densities $\rho(z)$ are normalized to electron density of water with buffer, $\rho_{subphase} = 0.339\ e^-/Å^{-3}$. (*b*) Illustration of one DPPC molecule and one GT_{1b} molecule in their approximate orientation at liquid surface. Two dashed lines represent average positions of alkyl tails/air interface ($z = 0$ Å) and center of headgroup region ($z \sim 20$ Å).

density (~20 Å) of the DPPC monolayer at 20 mN/m (Fig. 4 *b*) matches well with the value, $D_{HH}/2 = 21.4$ Å, previously measured in gel-phase DPPC bilayers (58).

Similar to the GT_{1b}/DPPE monolayer, a 20 mol % of GT_{1b} within a DPPC matrix provided sufficient spacing between GT_{1b} molecules laterally, and allowed the GT_{1b} saccharide region to assume full extension from the surface. When comparing monolayers of GT_{1b}/DPPC with GT_{1b}/DPPE, there was no difference in the electron density and length scale of the saccharide groups extending (20–25 Å) into the subphase. The main dissimilarity was in the electron density of the headgroups, very similar to the difference in electron density of pure DPPE and DPPC. However, in the case of GT_{1b}/DPPE, we observed a small decrease in headgroup electron density compared with pure DPPE. This observation is consistent with our in-plane GIXD data below. Again, based on reflectivity results there were no remarkable changes in the real-space structure at a surface pressure of 40 mN/m, except for a slight lengthening of the tail region, presumably because of a decrease in molecular tilt imposed by a decrease in area per molecule. There were also no significant structural changes with the equivalent monolayers at pH 5.

GIXD ANALYSIS

The GIXD measurements provided in-plane structural information on the ordered, diffracting portion of the monolayer. Diffraction from the alkyl tails was observed in the q_{xy} region ~1.1 to ~1.7 $Å^{-1}$, corresponding to *d*-spacings of ~5.7 to ~3.7 Å. No diffraction from the lipid headgroups (within a lower q_{xy} region) was detected. The Bragg peaks obtained for DPPE, 1:4 GT_{1b}/DPPE, DPPC, and 1:4 GT_{1b}/DPPC monolayers at pH 7.4 and 20 mN/m are shown in Fig. 5 *a*. The Bragg-rod profile for each monolayer is shown in Fig. 5 *b*. Analysis of the Bragg-rod profile was performed by approximating the lipid alkyl tails as tilted cylinders with length L_c and constant electron density (38).

For DPPE, three Bragg peaks were observed at $q_{xy} = 1.43$ $Å^{-1}$, $q_{xy} = 1.46$ $Å^{-1}$, and $q_{xy} = 1.49$ $Å^{-1}$. The presence of three Bragg peaks is indicative of an oblique 2D unit cell. The peaks can be indexed in a semihexagonal unit cell as {0, 1}, {1, 0}, and {1, −1}, respectively, similar to the findings of Wu et al. (59). The integrated intensities of Bragg peaks ($-0.05\ Å^{-1} \le q_z \le 0.9\ Å^{-1}$) were approximately the same, in agreement with the multiplicity rule. The observed Bragg peaks gave rise to a primitive 2D unit cell with dimensions of $|a| = 4.88$ Å, $|b| = 4.98$ Å, and $\gamma = 118.3°$, and an area per two alkyl chains of 42.74 $Å^2$. Similarly, for the 1:4 GT_{1b}/DPPE monolayer, the observed Bragg peaks gave rise to an oblique cell with dimensions of $|a| = 4.89$ Å, $|b| = 5.02$ Å, and $\gamma = 117.6°$, and an area per two alkyl chains of 43.47 $Å^2$. The GT_{1b}/DPPE monolayer exhibited a 1.7% increase in area per molecule, indicating that the presence of GT_{1b} caused slight packing inefficiencies in the ordered portion of the film. This expansion of the unit cell supports the idea that GT_{1b} is intercalated within the DPPE matrix, because all measurements were performed at constant surface pressure, and we observed no diffraction from pure GT_{1b}. If there were significant phase separation of the two components, the diffraction signal would have contained a component equivalent to pure DPPE. The Bragg-peak analysis is summarized in Table 1.

Bragg-rod analysis revealed a molecular tilt of 20.6° for DPPE and 24.0° for the GT_{1b}/DPPE monolayer. This increase in tilt of the lipid tails is consistent with the area-per-molecule increase shown by the shift to lower q_{xy} values for the Bragg peaks and a slight decrease in electron density of the headgroup (DPPE vs. GT_{1b}/DPPE) measured by reflectivity (Fig. 3 *b*). The other values obtained from the Bragg-rod analysis were $L_c \approx 18$ Å and $\sigma \approx 1.5$ Å, and the tilt directions for DPPC and DPPE were approximately toward their nearest neighbor ($a + b$ direction; Fig. 5 *c*). The tilt directions for the mixtures (GT_{1b}/DPPE and GT_{1b}/DPPC) slightly deviated from those of their nearest neighbor, which resulted in additional distortion of the unit cell, from distorted

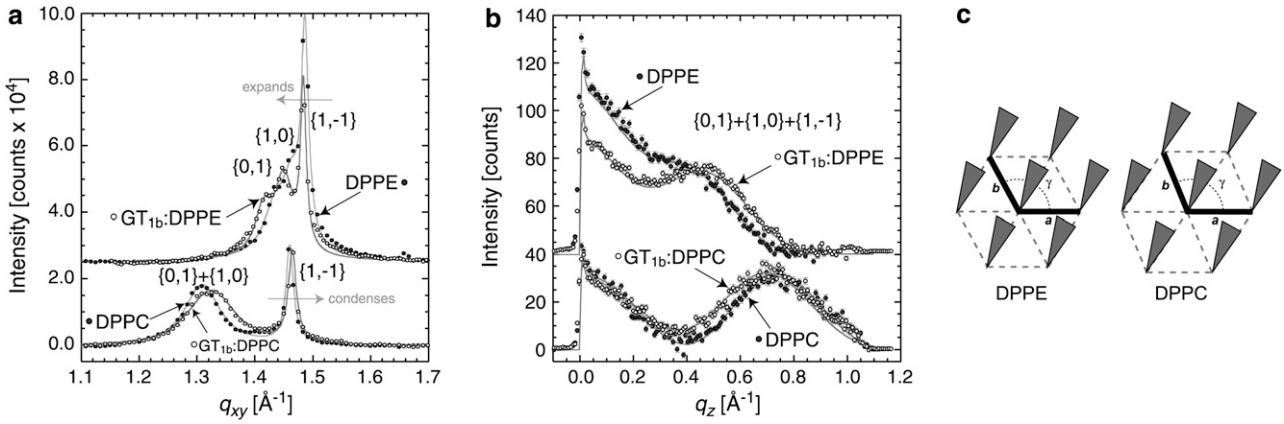

FIGURE 5 Grazing-incidence x-ray diffraction from ordered alkyl tail regions of DPPE, GT_{1b}/DPPE, DPPC, and GT_{1b}/DPPC monolayers. (*a*) Bragg peaks. (*b*) Bragg rods. The DPPE and GT_{1b}/DPPE data are offset from DPPC and GT_{1b}/DPPC data in each case for clarity. The three GIXD Bragg peaks indicate packing of the lipid tails in an oblique 2D unit cell. Miller indices of each peak are provided. (*a*) Gray arrows highlight unit-cell expanding for GT_{1b}/DPPE monolayer, and condenseing for GT_{1b}/DPPC monolayer. Bragg peaks were fit using Voight functions (*solid gray lines*). (*b*) Bragg rods were fitted (*solid line*) by approximating the coherently scattering part of the alkyl tail by a cylinder with length L_c and constant electron density. The sharp peak at $q_z = 0.01$ Å^{-1} is so-called Yoneda-Vineyard peak (66), which arises from interference between x-rays diffracted up into a monolayer and x-rays diffracted down and then reflected up by interface. (*c*) Top view of arrangement of hydrocarbon tails of DPPE and DPPC molecules within unit cells at 20 mN/m. Their azimuthal tilt direction is approximately along the $a + b$ direction, and molecules are tilted from surface normal by angles indicated in the text.

hexagonal to oblique (especially visible in the case of GT_{1b}/DPPE, where three Bragg peaks are evident). There were no remarkable changes to the in-plane packing at a surface pressure of 40 mN/m, except for an expected decrease in molecular tilt (~0°) and area per molecule (~40.36 Å^2). Because the data reported here use a monolayer at 20 mN/m as a model membrane, there was a large difference in the tilt angle of DPPE hydrocarbon tails (20.6°) compared with previous observations of zero tilt in phosphatidylethanolamine bilayers (60–63). This discrepancy is a result of the relatively larger area per molecule imposed on the monolayers at 20 mN/m. At 40 mN/m, the hydrocarbon tails had hexagonal packing, indicated by one Bragg peak, and were not tilted.

For DPPC, two Bragg peaks were observed at $q_{xy} = 1.31$ Å^{-1} and $q_{xy} = 1.46$ Å^{-1}. The presence of two Bragg peaks is indicative of a distorted hexagonal 2D cell with $|a| = |b|$ and $\gamma \neq 120$, with the Miller indices $\{(0,1),(1,0)\}$ and $\{1,-1\}$. The observed Bragg peaks give rise to a primitive 2D unit cell with dimensions of $|a| = 5.19$ Å, $|b| = 5.19$ Å, and $\gamma = 112.2°$, and an area per two alkyl chains of 49.80 Å^2. This area per molecule matches reasonably well with previous gel-phase DPPC bilayer work (49,64). The small discrepancy is attributable to the monolayer's surface pressure of 20 mN/m. Similarly for the 1:4 GT_{1b}/DPPC monolayer, the observed Bragg peaks give rise to a primitive 2D unit cell with dimensions of $|a| = 5.15$ Å, $|b| = 5.15$ Å, and $\gamma = 112.9°$, and an area per two alkyl chains of 48.87 Å^2. In contrast to the GT_{1b}/DPPE monolayer, the GT_{1b}/DPPC system exhibited a 1.9% decrease in area per molecule, indicating that the presence of GT_{1b} caused a slight condensing effect in the ordered portion of the film. This observation is consistent with isotherm results. A similar condensing effect was observed in previous work for GM_1/DPPC monolayers (51). Condensing of the unit cell supports the idea that GT_{1b} is intercalated within the DPPC matrix, because all measurements were performed at constant surface pressure, and we observed no diffraction from pure GT_{1b}. If there were phase separation of the two components, the diffraction signal would have contained a component equivalent to pure DPPC.

Bragg-rod analysis revealed a molecular tilt of 35.3° for DPPC and 33.5° for the GT_{1b}/DPPC monolayer. This decrease in tilt of the lipid tails is consistent with the area-per-molecule decrease shown by the shift to larger q_{xy} values for the Bragg peaks.

TABLE 1 In-plane structural parameters obtained from GIXD analysis

	In-plane Bragg Peaks			
Composition: $\pi = 20$ mN/m, pH = 7.4	a, b (Å) ± 0.002 (Å)	γ (°) ± 0.2 (°)	Area per molecule (Å^2) ± 0.04	In-plane coherence length L_{xy} ± 10.0 (Å)
DPPE	4.877 4.976	118.3	42.74	120, 145, 460
GT_{1b}/DPPE	4.892 5.015	117.6	43.47	170, 145, 700
DPPC	5.186 5.186	112.2	49.80	80,* 410
GT_{1b}/DPPC	5.150 5.150	112.9	48.87	60,* 390

*Large uncertainty because {0,1} and {1,0} Bragg peaks could not be resolved separately.

DISCUSSION AND CONCLUSIONS

Our x-ray scattering measurements revealed that pure GT_{1b} can form a stable monolayer up to a surface pressure of ~35

mN/m, but there was no observable in-plane ordering of its alkyl tails. The XR showed that the total out-of-plane length of pure GT_{1b} is much shorter than expected from its chemical structure, probably because of the ''coil-like'' conformation of the saccharide group at 20 mN/m. This reveals that pure GT_{1b} is not a suitable model membrane for studying interactions with proteins. However, at 20 mol %, GT_{1b} can be fully integrated within a host DPPE or DPPC monolayer matrix at surface pressures of 20 and 40 mN/m and pH values of 7.4 and 5. For these mixtures and surface pressures, the GT_{1b} saccharide groups were clearly visible, extending ~20 Å into the liquid subphase from the phospholipid headgroups. These finding are analogous to earlier work with 30 mol % GM_1 in egg PC bilayers, where the GM_1 headgroups exhibited full extension into the aqueous phase (65). The saccharide region of pure GT_{1b} exhibits a measured electron density of $1.26\rho_{subphase}$ (measured at a depth of 20 Å; Fig. 3 *b*), similar to the value of the DPPC headgroup. In the GT_{1b} mixture with DPPE or DPPC, one would expect the density of the saccharide region to be $1.05\rho_{subphase} = (0.20(1.26\rho_{subphase} - \rho_{subphase}) + \rho_{subphase})$, according to the molar ratio of the components and the measured electron density of the saccharide region of pure GT_{1b}. The observed electron density of the saccharide region in the mixture is $1.20\rho_{subphase}$ (measured at a depth of ~35Å; Fig. 3 *b*), much larger than the expected value. This is most likely due to a lack of hydration in the case of pure GT_{1b}, associated with the ''coil-like'' conformation, which could enhance the interaction between neighboring saccharide groups, limiting the access of water molecules. Within the GT_{1b} mixtures, the spacing between adjacent saccharide groups provided by the lipid matrix enables full hydration of the saccharide region, and therefore measured electron density increases.

Grazing-incidence x-ray diffraction shows that the incorporation of 20 mol % GT_{1b} does not substantially alter the in-plane packing of DPPE and DPPC. Because of the very high packing efficiencies of pure DPPE (relative to pure DPPC because of the larger phosphatidylcholine headgroup volume (48,55)), GT_{1b} incorporation caused an increase in area per molecule (+1.7%). However, when GT_{1b} was incorporated with DPPC, there was a slight but measurable decrease (−1.9%) in area per molecule.

One of the goals in characterizing GT_{1b}/DPPE and GT_{1b}/DPPC was to find indications of whether phase separation of the two components occurred in each monolayer system. Using outcomes from x-ray reflectivity, GIXD, and pressure-area isotherms, we observed no evidence to support significant phase separation. The GIXD from GT_{1b}/DPPE and GT_{1b}/DPPC exhibited different unit-cell parameters than did pure DPPE and DPPC, respectively. If complete phase separation had occurred, we would expect scattering equivalent to that of pure DPPE/DPPC, because we observed no scattering from pure GT_{1b}. Finally, pressure-area isotherms showed no signs of phase separation, in that no isotherm results showed a linear combination of isotherms of the pure components. All three pieces of evidence support the idea that GT_{1b} is intercalated well with DPPE/DPPC, and does not significantly separate into discrete domains.

In both cases, the oligosaccharide headgroups extended normally from the monolayer surfaces into the subphase, with full access to the water environment. Our study demonstrated that these monolayers are stable at up to 20 mol % of GT_{1b}. This relatively high concentration of GT_{1b} will maximize interactions of proteins that associate with GT_{1b}, making these monolayers an ideal platform for investigating toxin membrane-binding and penetration.

D.D.B is grateful to Bal Ram Singh for helpful discussions, and to Brigham Young University for sabbatical support for this project. B.S. acknowledges the contributions to this work of travel support from Brigham Young University and Los Alamos National Laboratory (LANL). We also thank HASYLAB for beamtime. We thank Dr. K. Kjaer for help with the monolayer scattering experiments.

The Los Alamos Neutron Science Center at the Los Alamos National Laboratory is funded by the United States Department of Energy under contract W-7405-ENG-36. J.M and C.E.M. thank the LANL-Laboratory Directed Research and Development program of the Department of Energy's Office of Science (Basic Energy Sciences) for financial support. C.E.M. acknowledges support from the LANL Director's Post-Doctoral Fellowship and the Institute for Complex Adaptive Matter.

REFERENCES

1. Maggio, B., M. L. Fanani, C. M. Rosetti, and N. Wilke. 2006. Biophysics of sphingolipids II. Glycosphingolipids: an assortment of multiple structural information transducers at the membrane surface. *Biochim. Biophys. Acta.* 1758:1922–1944.
2. Thiesen, P. H., H. Rosenfeld, P. Konidala, V. M. Garamus, L. He, A. Prange, and B. Niemeyer. 2006. Glycolipids from a colloid chemical point of view. *J. Biotechnol.* 124:284–301.
3. Levery, S. B. 2005. Glycosphingolipid structural analysis and glycosphingolipidomics. *Methods Enzymol.* 405:300–369.
4. Svennerholm, L. 1963. Chromatographic separation of human brain gangliosides. *J. Neurochem.* 10:613–623.
5. Sonnino, S., L. Cantù, M. Corti, D. Acquotti, and B. Venerando. 1994. Aggregative properties of gangliosides in solution. *Chem. Phys. Lipids.* 71:21–45.
6. Smith, R., and C. Tanford. 1972. The critical micelle concentration of L-alpha-dipalmitoylphosphatidylcholine in water and water-methanol solutions. *J. Mol. Biol.* 69:75–83.
7. Ayuyan, A. G., and F. S. Cohen. 2008. Raft composition at physiological temperature and pH in the absence of detergents. *Biophys. J.* 94:2654–2666.
8. Angata, T., and A. Varki. 2000. Siglec-7: a sialic acid-binding lectin of the immunoglobulin superfamily. *Glycobiology.* 10:431–438.
9. Avril, T., H. Floyd, F. Lopez, E. Vivier, and P. R. Crocker. 2004. The membrane-proximal immunoreceptor tyrosine-based inhibitory motif is critical for the inhibitory signaling mediated by Siglecs-7 and -9, CD33-related Siglecs expressed on human monocytes and NK cells. *J. Immunol.* 173:6841–6849.
10. Falco, M., R. Biassoni, C. Bottino, M. Vitale, S. Sivori, R. Augugliaro, L. Moretta, and A. Moretta. 1999. Identification and molecular cloning of p75/AIRM1, a novel member of the sialoadhesin family that functions as an inhibitory receptor in human natural killer cells. *J. Exp. Med.* 190:793–802.
11. Hakomori, S. 1990. Bifunctional role of glycosphingolipids. Modulators for transmembrane signaling and mediators for cellular interactions. *J. Biol. Chem.* 265:18713–18716.

12. Hakomori, S. 1996. Tumor malignancy defined by aberrant glycosylation and sphingo(glyco)lipid metabolism. *Cancer Res.* 56:5309–5318.

13. Hakomori, S. 1998. Cancer-associated glycosphingolipid antigens: their structure, organization, and function. *Acta Anat. (Basel).* 161: 79–90.

14. Hakomori, S., and Y. Igarashi. 1995. Functional role of glycosphingolipids in cell recognition and signaling. *J. Biochem. (Tokyo).* 118: 1091–1103.

15. Ikehara, Y., S. K. Ikehara, and J. C. Paulson. 2004. Negative regulation of T cell receptor signaling by Siglec-7 (p70/AIRM) and Siglec-9. *J. Biol. Chem.* 279:43117–43125.

16. Nicoll, G., J. Ni, D. Liu, P. Klenerman, J. Munday, S. Dubock, M. G. Mattei, and P. R. Crocker. 1999. Identification and characterization of a novel Siglec, Siglec-7, expressed by human natural killer cells and monocytes. *J. Biol. Chem.* 274:34089–34095.

17. Vyas, A. A., and R. L. Schnaar. 2001. Brain gangliosides: functional ligands for myelin stability and the control of nerve regeneration. *Biochimie.* 83:677–682.

18. Schnaar, R. L., B. E. Collins, L. P. Wright, M. Kiso, M. B. Tropak, J. C. Roder, and P. R. Crocker. 1998. Myelin-associated glycoprotein binding to gangliosides. Structural specificity and functional implications. *Ann. N. Y. Acad. Sci.* 845:92–105.

19. Barclay, W. S., I. M. Jones, H. M. Osborn, L. Phillipson, J. Ren, G. A. Talevera, and C. I. Thompson. 2007. Probing the receptor interactions of an H5 avian influenza virus using a baculovirus expression system and functionalised poly(acrylic acid) ligands. *Bioorg. Med. Chem.* 15:4038–4047.

20. Matrosovich, M. N., A. S. Gambaryan, S. Teneberg, V. E. Piskarev, S. S. Yamnikova, D. K. Lvov, J. S. Robertson, and K. A. Karlsson. 1997. Avian influenza A viruses differ from human viruses by recognition of sialyloligosaccharides and gangliosides and by a higher conservation of the HA receptor-binding site. *Virology.* 233:224–234.

21. Nayak, D. P., E. K. Hui, and S. Barman. 2004. Assembly and budding of influenza virus. *Virus Res.* 106:147–165.

22. Teissier, E., and E. I. Pécheur. 2007. Lipids as modulators of membrane fusion mediated by viral fusion proteins. *Eur. Biophys. J.* 36: 887–899.

23. Lauer, S., B. Goldstein, R. L. Nolan, and J. P. Nolan. 2002. Analysis of cholera toxin-ganglioside interactions by flow cytometry. *Biochemistry.* 41:1742–1751.

24. Ribi, H. O., D. S. Ludwig, K. L. Mercer, G. K. Schoolnik, and R. D. Kornberg. 1988. 3-Dimensional structure of cholera-toxin penetrating a lipid-membrane. *Science.* 239:1272–1276.

25. Venienbryan, C., P. F. Lenne, C. Zakri, A. Renault, A. Brisson, J. F. Legrand, and B. Berge. 1998. Characterization of the growth of 2D protein crystals on a lipid monolayer by ellipsometry and rigidity measurements coupled to electron microscopy. *Biophys. J.* 74:2649–2657.

26. Bohnert, S., K. Deinhardt, S. Salinas, and G. Schiavo. 2006. Uptake and transport of clostridium neurotoxins. *In* The Sourcebook of Comprehensive Bacterial Protein Toxins. J. E. Alouf and M. R. Popoff, editors. Elsevier, Amsterdam. 390–408.

27. Couesnon, A., Y. Pereira, and M. R. Popoff. 2007. Receptor-mediated transcytosis of botulinum neurotoxin A through intestinal cell monolayers. *Cell Microbiol.* 10:375–387.

28. Kitamura, M., K. Takamiya, S. Aizawa, and K. Furukawa. 1999. Gangliosides are the binding substances in neural cells for tetanus and botulinum toxins in mice. *Biochim. Biophys. Acta.* 1441:1–3.

29. Kohda, T., H. Ihara, Y. Seto, H. Tsutsuki, M. Mukamoto, and S. Kozaki. 2007. Differential contribution of the residues in C-terminal half of the heavy chain of botulinum neurotoxin type B to its binding to the ganglioside GT1b and the synaptotagmin 2/GT1b complex. *Microb. Pathog.* 42:72–79.

30. Kozaki, S., Y. Kamata, S. Watarai, T. Nishiki, and S. Mochida. 1998. Ganglioside GT1b as a complementary receptor component for *Clostridium botulinum* neurotoxins. *Microb. Pathog.* 25:91–99.

31. Montecucco, C., O. Rossetto, and G. and Schiavo. 2004. Presynaptic receptor arrays for clostridial neurotoxins. *Trends Microbiol.* 12: 442–446.

32. Nishiki, T., Y. Tokuyama, Y. Kamata, Y. Nemoto, A. Yoshida, K. Sato, M. Sekiguchi, M. Takahashi, and S. Kozaki. 1996. The high-affinity of *Clostridium botulinum* type B neurotoxin to synaptotagmin II associated with gangliosides GT1B/GD1a. *FEBS Lett.* 378:253–257.

33. Rossetto, O., and C. Montecucco. 2007. Peculiar binding of botulinum neurotoxin. *ACS Chem. Biol.* 2:96–98.

34. Schiavo, G. 2006. Structural biology: dangerous liaisons on neurons. *Nature.* 444:1019–1020.

35. Yowler, B. C., and C. L. Schengrund. 2004. Botulinum neurotoxin A changes conformation upon binding to ganglioside GT1b. *Biochemistry.* 43:9725–9731.

36. Majewski, J., T. L. Kuhl, K. Kjær, and G. S. Smith. 2001. Packing of ganglioside-phospholipid monolayers: an X-ray diffraction and reflectivity study. *Biophys. J.* 81:2707–2715.

37. Miller, C. E., J. Majewski, R. Faller, S. Satija, and T. L. Kuhl. 2004. Cholera toxin assault on lipid monolayers containing ganglioside GM1. *Biophys. J.* 86:3700–3708.

38. Als-Nielsen, J., D. Jacquemain, K. Kjaer, F. Leveiller, M. Lahav, and L. Leiserowitz. 1994. Principles and applications of grazing incidence x-ray and neutron scattering from ordered molecular monolayers at the air-water interface. *Phys. Rep.* 246:252–313 [review].

39. Kjaer, K., J. Alsnielsen, C. A. Helm, P. Tippmannkrayer, and H. Mohwald. 1988. An x-ray-scattering study of lipid monolayers at the air water interface and on solid supports. *Thin Solid Films.* 159:17–28.

40. Jensen, T. R., and K. Kjaer. 2001. Novel methods to study interfacial layers: structural properties and interactions of thin films at the air-liquid interface explored by synchrotron x-ray scattering. *In* Studies in Interface Science. D. Möbius and R. Miller, editors. Elsevier, Amsterdam. 205–254.

41. Kjaer, K. 1994. Some simple ideas on x-ray reflection and grazing-incidence diffraction from thin surfactant films. *Physica B (Amsterdam).* 198:100–109.

42. Miller, C. E., J. Majewski, T. Gog, and T. L. Kuhl. 2005. Grazing incidence diffraction of cadmium arachidate multilayers at the solid-liquid interface. *Zeitschrift Fur Kristallographie.* 220:987–992.

43. Pedersen, J. S., and I. W. Hamley. 1994. Analysis of neutron and x-ray reflectivity data by constrained least-squares methods. *Physica B (Amsterdam).* 198:16–23.

44. Pedersen, J. S., and I. W. Hamley. 1994. Analysis of neutron and X-ray reflectivity data. I. Theory. *J. Appl. Cryst.* 27:29–35.

45. Pedersen, J. S., and I. W. Hamley. 1994. Analysis of neutron and X-ray reflectivity data. II. Constrained least-squares methods. *J. Appl. Cryst.* 27:36–49.

46. Li, C. H., D. Constantin, and T. Salditt. 2004. Biomimetic membranes of lipid-peptide model systems prepared on solid support. *J. Phys. Condens. Matter.* 16:S2439–S2453.

47. Spaar, A., C. Munster, and T. Salditt. 2004. Conformation of peptides in lipid membranes studied by x-ray grazing incidence scattering. *Biophys. J.* 87:396–407.

48. Tristram-Nagle, S., Y. F. Liu, J. Legleiter, and J. F. Nagle. 2002. Structure of gel phase DMPC determined by x-ray diffraction. *Biophys. J.* 83:3324–3335.

49. Tristram-Nagle, S., R. Zhang, R. M. Suter, C. R. Worthington, W. J. Sun, and J. F. Nagle. 1993. Measurement of chain tilt angle in fully hydrated bilayers of gel phase lecithins. *Biophys. J.* 64:1097–1109.

50. Gopal, A., and K. Y. C. Lee. 2006. Headgroup percolation and collapse of condensed Langmuir monolayers. *J. Phys. Chem. B.* 110:22079–22087.

51. Frey, S. L., E. Y. Chi, C. Arratia, J. Majewski, K. Kjaer, and K. Y. C. Lee. 2008. Condensing and fluidizing effects of ganglioside GM1 on phospholipid films. *Biophys. J.* 94:3047–3064.

52. Helm, C. A., H. Möhwald, K. Kjaer, and J. Als-Nielsen. 1987. Phospholipid monolayers between fluid and solid states. *Biophys. J.* 52:381–390.

53. Helm, C. A., P. Tippmannkrayer, H. Möhwald, J. Als-Nielsen, and K. Kjaer. 1991. Phases of phosphatidyl ethanolamine monolayers studied by synchrotron x-ray-scattering. *Biophys. J.* 60:1457–1476.

54. Small, D. M. 1967. Phase equilibria and structure of dry and hydrated egg lecithin. *J. Lipid Res.* 8:551–557.

55. Nagle, J. F., and S. Tristram-Nagle. 2000. Structure of lipid bilayers. *Biochim. Biophys. Acta.* 1469:159–195.

56. Reference deleted in proof.

57. Janiak, M. J., D. M. Small, and G. G. Shipley. 1976. Nature of thermal pre-transition of synthetic phospholipids—dimyristoyllecithin and dipalmitoyllecithin. *Biochemistry.* 15:4575–4580.

58. Sun, W. J., S. Tristram Nagle, R. M. Suter, and J. F. Nagle. 1996. Structure of gel phase saturated lecithin bilayers: temperature and chain length dependence. *Biophys. J.* 71:885–891.

59. Wu, G. H., J. Majewski, C. Ege, K. Kjaer, M. J. Weygand, and K. Y. C. Lee. 2005. Interaction between lipid monolayers and poloxamer 188: an x-ray reflectivity and diffraction study. *Biophys. J.* 89:3159–3173.

60. Hauser, H., I. Pascher, R. H. Pearson, and S. Sundell. 1981. Preferred conformation and molecular packing of phosphatidylethanolamine and phosphatidylcholine. *Biochim. Biophys. Acta.* 650:21–51.

61. Mcintosh, T. J. 1980. Differences in hydrocarbon chain tilt between hydrated phosphatidylethanolamine and phosphatidylcholine bilayers—molecular packing model. *Biophys. J.* 29:237–245.

62. Miller, C. E., J. Majewski, E. B. Watkins, D. J. Mulder, T. Gog, and T. L. Kuhl. 2008. Probing the local order of single phospholipid membranes using grazing incidence x-ray diffraction. *Phys. Rev. Lett.* 100:058103.

63. Tenchov, B., R. Koynova, and G. Rapp. 2001. New ordered metastable phases between the gel and subgel phases in hydrated phospholipids. *Biophys. J.* 80:1873–1890.

64. Sun, W. J., R. M. Suter, M. A. Knewtson, C. R. Worthington, S. Tristramnagle, R. Zhang, and J. F. Nagle. 1994. Order and disorder in fully hydrated unoriented bilayers of gel phase dipalmitoylphosphatidylcholine. *Phys. Rev. E Stat. Phys. Plasmas Fluids Relat. Interdiscip. Topics.* 49:4665–4676.

65. Mcintosh, T. J., and S. A. Simon. 1994. Long-range and short-range interactions between phospholipid/ganglioside Gm1 bilayers. *Biochemistry.* 33:10477–10486.

66. Vineyard, G. H. 1982. Grazing-incidence diffraction and the distorted-wave approximation for the study of surfaces. *Phys. Rev. B.* 26:4146–4159.